

Efficient Phase Estimation for Interferogram Stacks

Homa Ansari^{ID}, Francesco De Zan^{ID}, and Richard Bamler^{ID}, *Fellow, IEEE*

Abstract—Signal decorrelation poses a limitation to multipass SAR interferometry. In pursuit of overcoming this limitation to achieve high-precision deformation estimates, different techniques have been developed, with short baseline subset, SqueeSAR, and CAESAR as the overarching schemes. These different analysis approaches raise the question of their efficiency and limitation in phase and consequently deformation estimation. This contribution first addresses this question and then proposes a new estimator with improved performance, called Eigendecomposition-based Maximum-likelihood-estimator of Interferometric phase (EMI). The proposed estimator combines the advantages of the state-of-the-art techniques. Identical to CAESAR, EMI is solved using eigendecomposition; it is therefore computationally efficient and straightforward in implementation. Similar to SqueeSAR, EMI is a maximum-likelihood-estimator; hence, it retains estimation efficiency. The computational and estimation efficiency of EMI renders it as an optimum choice for phase estimation. A further marriage of EMI with the proposed Sequential Estimator by Ansari *et al.* provides an efficient processing scheme tailored to the analysis of Big InSAR Data. EMI is formulated and verified in relation to the state-of-the-art approaches via mathematical formulation, simulation analysis, and experiments with time series of Sentinel-1 data over the volcanic island of Vulcano, Italy.

Index Terms—Big Data, coherence matrix, covariance estimation, differential interferometric synthetic aperture radar, distributed scatterers (DS), efficiency, error analysis, maximum-likelihood estimation, near real-time (NRT) processing.

NOMENCLATURE

CCG	Complex circular gaussian.
CRLB	Cramér–Rao lower bound.
DS	Distributed scatterers.
EVD	Eigenvalue decomposition.
InSAR	Interferometric SAR.
MLE	Maximum likelihood estimator.
NRT	Near real-time.
PDF	Probability density function.
EMI	Eigendecomposition-based Maximum-likelihood-estimator of Interferometric phase.
PL	Phase linking.
PS	Persistent scatterers.

Manuscript received November 28, 2017; revised February 15, 2018; accepted April 7, 2018. Date of publication May 24, 2018; date of current version June 22, 2018. This work was supported by the German Helmholtz Alliance on Remote Sensing and Earth System Dynamics. (*Corresponding author:* Homa Ansari.)

H. Ansari and F. De Zan are with the German Aerospace Center, 82234 Weßling, Germany (e-mail: homa.ansari@dlr.de).

R. Bamler is with the German Aerospace Center, Remote Sensing Technology Institute, 82234 Weßling, Germany, and also with the Chair of Remote Sensing Technology, Technical University of Munich, 80333 Munich, Germany.

Color versions of one or more of the figures in this paper are available online at <http://ieeexplore.ieee.org>.

Digital Object Identifier 10.1109/TGRS.2018.2826045

PSI	Persistent scatterer interferometry.
PTA	Phase triangulation algorithm.
RMSE	Root mean square error.
SAR	Synthetic aperture radar.
SCM	Sample correlation matrix.
SLC	Single look complex.

I. INTRODUCTION

INTERFEROMETRIC analysis of multitemporal SAR data has proven to be a powerful technique in geodetic monitoring of the Earth surface deformation. The interferometric phase between two SAR acquisitions comprises a systematic component corrupted by a stochastic noise. The former is attributed to the variation of the optical path between the SAR sensor and the sensed area [2] and caused for instance by deformation and atmospheric-induced range variation [3]. The latter is related to abrupt alteration or stochastic position/property changes of the subresolution scatterers and causes decorrelation of the SAR signal between two acquisitions [4]. The focus of InSAR time series analysis techniques has been dedicated to tackling the signal decorrelation as well as the separation of the deformation and atmospheric signal. The first breakthrough in this regard was the introduction of PSI technique [5], [6]. In tackling the decorrelation, the technique bounds the estimation of systemic signal to PSs. PS are phase-stable scatterers, which undergo minor decorrelation in the time series. PSI was later generalized by the relaxation of the limit on the stability of the scatterers and exploiting DSs. DS are natural scatterers distributed over an area larger than PS that undergo coherence loss in the time series. To overcome the decorrelation, DS techniques either limit the analysis to moderate coherent interferograms to high coherent interferograms or estimate the systematic phase behavior by incorporation of all possible interferograms relative to their statistical characteristics. The former approach is known as the Short Baseline Subset (SBAS) technique [7]; the latter is pioneered by the PTA [8], [9], and its further variations are introduced by EVD [10]–[12]. After the pioneering authors, the estimation of systematic phase series from all possible interferograms is hereafter referred to as PL. The difference between PL and SBAS is in the full versus partial exploitation of the abundance of interferograms. As statistically expected, the exploitation of all even weakly coherent interferograms in PL improves the signal-to-noise ratio (SNR) in phase estimation and consequently enhances the sensitivity to mm-level deformation estimation. Furthermore, PL is theoretically expected to decrease the estimation bias in the presence of phase inconsistencies [13], [14].

The PL techniques are mathematically compared in [15]. Here, the authors interpret the difference of PL approaches

in terms of the adopted weighting strategy for incorporation of the interferograms. These various weighting strategies raise the question of the optimum approach for PL. This question is addressed by the CRLB of phase estimation in [16]. Theoretically, the weighting considered by PTA is the optimum choice for PL. Imposing the phase consistency [9], [13], PTA introduces a model for PL. The model is fitted to the interferometric data in an MLE formulation. The MLE is asymptotically the closest estimator to the CRLB. Therefore, under the validity of the assumptions of PTA, it provides the optimum solution to the retrieval of the sought systematic phase series. However, the violation of these assumptions compromises this optimum performance [1], [17]–[19]. One such assumption is the sufficiency of the data covariance, estimated empirically, to describe data statistics. The latter estimator is, however, known to be erroneous, especially for small ensembles and covariance close to zero [20], [21]. The performance of PTA is known and shown to be severely degraded in such cases [1], [2], [18], [19]. However, the occurrence of such extreme scenarios is rare and detectable in postprocessing. In this specific case, the heuristic weighting strategy introduced in [22] may substitute the optimum weighting to marginally improve the performance. Despite this disadvantage, PTA provides a data-adaptive time series analysis technique tailored to mm-level deformation monitoring. Therefore, it fulfills the demand for an optimum analysis technique for the interferometric time series.

The recent launch and planning of global monitoring wide-swath SAR missions provide an unprecedented wealth of data. The exploitation of the emerging Big Data entails a new demand on the computational efficiency of the time series analysis techniques. On the one hand, the exploitation of all interferometric pairs in an MLE framework increases the estimation efficiency in deformation monitoring. On the other hand, this processing scheme is computationally demanding, pitting the estimation efficiency against the computational efficiency. One attitude toward managing the challenges of Big Data is to resort to parallel computing and exploitation of a mere selection of the interferometric data in the framework of SBAS [23]. A second attitude is to migrate from the conventional state-of-the-art algorithms and invest in alternative estimators to exploit the wealth of data as far as possible (the role of full exploitation of data is twofold: first, it improves the SNR in phase estimation and consequently enhances the sensitivity to mm-level deformation estimation; second, it is theoretically expected to decrease the estimation bias in the presence of phase inconsistencies [13], [14]). The design criterion for the alternative estimators shall be the optimization of the tradeoff between the estimation and computational efficiency. A marriage of such alternative estimators with the parallel computing capabilities is an obvious further step toward a fully optimized processing scheme tailored to efficient Big Data mining.

The recent proposal of Sequential Estimator [1] moves toward optimized algorithms for NRT processing of the Big Data. In the interest of improving the computational efficiency, this estimator divides the time series into isolated small data batches, processes them in turn with the PTA, and finally

compresses each batch. In retaining the estimation efficiency, it retrieves the lost interferometric signal among the isolated batches via the formation of the so-called artificial interferograms and incorporates them in the phase estimation. Although successful in reducing both the computational burden and the demanding data storage capacity of the Big Data under process, the core PTA of the Sequential Estimator is still a performance bottleneck for NRT data processing both in terms of computation and estimation efficiency.

The focus of this paper is to revisit PL and put forward an alternative estimator with an improved efficiency. The proposed estimator generalizes the PTA model for PL. Following the generalized model, it pursues the maximization of the resulted likelihood probability. In the interest of retaining computational efficiency, the reference MLE is approximated and constrained. With these interventions, the generalized PL is transformed to an optimization with equality constraint and is formulated in a Lagrangian. The latter is efficiently solved by eigendecomposition. The proposed generalized PL is termed EMI to best capture the mathematical background behind its derivation.

The incentive behind the generalization of the PTA model by EMI is to allow extra degrees of freedom to the estimator for the calibration of the employed covariance as the data statistics. In the absence of covariance estimation error, the two models converge and the two estimators are equivalent. In the presence of this error, EMI is expected to improve the estimation efficiency. Besides the proposal of a new PL approach, this paper contributes to advancing the understanding of PL approaches by the following:

- 1) mathematical comparison of PTA, EVD, and EMI estimators and interpretation of their difference in terms of factorization of the covariance matrix;
- 2) formulation of the MLE for PL and showing that both PTA and EMI are approximations of the MLE based on different assumptions;
- 3) analysis of the estimation and computational efficiency of the three estimators;
- 4) revisiting PTA and its efficient numerical solution proposed in [8];
- 5) highlighting the impact of initialization on the numerical solution of PTA;
- 6) investigation of the convergence behavior of PTA;
- 7) validating the computational and estimation efficiency of EMI, in support of its selection as an optimum choice for Big Data processing.

In the continuation of this paper, the different approaches to PL are reviewed, and their distinction is mathematically interpreted. EMI is formulated and compared in relation to these state-of-the-art approaches via mathematical formulation, simulation analysis, and experiments with time series of Sentinel-1 data, in Sections II–IV, respectively.

II. EMI: A PROPOSAL FOR EFFICIENT PL

A. State-of-the-Art PL Approaches

PL aims at the estimation of a common-master interferometric phase series from all possible interferograms in a time series of the SAR data. That is, having n coregistered

SAR images, PL estimates $n - 1$ independent phase values from the $n(n - 1)/2$ interferograms. The estimated phase series is relative to an arbitrary master. It pertains to a systematic phase between the master and slave, induced by the variation in the optical path of the sensor to the scatterers [2]. Thus, the systematic phase is attributed to the superimposition of atmospheric, topographic, and geophysical changes [4]. Similar to PSI, the isolation of the geophysical signal from the latter systematic effects follows in a separate estimation step [2], [8], [9].

To commence with the formulation of PL, let us consider a statistically homogeneous region of Ω of l pixels in a time series of n SAR images, arranged in a matrix $Z \in \mathbb{C}^{n \times l}$, where l refers to the spatial domain and n refers to the temporal domain; Z is therefore a spatio-temporal aggregation of the pixels of the Ω region. Based on the central limit theorem, Z follows the zero-mean n -variate CCG distribution [21], [24]. Under the assumption of validity of this distribution, the second moment of the data suffices for the description of its statistics. The sample covariance matrix, or its normalized version SCM, is known to be the MLE of the second-order moment [24]. The SCM is given by

$$C = \frac{ZZ^H}{\sqrt{\|Z\|^2 (\|Z\|^2)^T}} \quad (1)$$

where $.^H$ indicates the Hermitian conjugation, $\|Z\|$ gives the rowwise L2 norm of the matrix Z , and the power-2 and division operations are elementwise. Under the assumption of validity of CCG, the SCM is a concise and sufficient descriptor of SAR data. Allowing the decomposition of the complex SCM to its *elementwise* modulus and argument

$$\begin{aligned} C &= |C| \circ I_\Omega = \Gamma \circ I_\Omega \\ \text{with } (I_\Omega)_{ik} &= \exp(j\Delta\phi_{ik}) \end{aligned} \quad (2)$$

where \circ is the Hadamard product. In this decomposition, Γ indicates the signal coherence between the corresponding images in the stack; it is hereafter referred to as the coherence matrix. I_Ω contains the spatially estimated interferograms obtained by averaging over the Ω ensemble. They pertain to the sought systematic phase and are, however, corrupted by SCM estimation variance and temporal decorrelation. PL is an additional estimator, designed to improve the spatial estimation of this systematic phase signature by the exploitation of data statistics in the temporal direction. Different PL approaches consider different matrix factorizations in modeling the SCM.

1) PTA Approach to PL: It introduces Σ as a model for the underlying covariance, or better correlation, of an n -variate CCG process. It further proposes a factorization of this matrix to two complex diagonals (Ψ) and one full-rank real-symmetric matrix (Γ) [8], [9]

$$\begin{aligned} \text{with } \Gamma &\in \mathbb{R}^{n \times n} \\ \text{and } \Psi &= \text{diag}[\psi] = \text{diag}[\exp(j\phi_i)] \\ \Sigma &= \Psi\Gamma\Psi^H = \Gamma \circ \psi\psi^H. \end{aligned} \quad (3)$$

It further assumes that the coherence provides a sufficient estimation of Γ and allows $\hat{\Gamma}_{ik} = |\Gamma_{ik}|$. In so doing, PTA assumes the estimated coherence to be of high precision and accuracy and is limited to estimating the phase series in ψ .

2) EVD Approach to PL: It proposes a different factorization to two full-rank complex matrices (V), forming an orthonormal basis, and one diagonal real matrix (Λ)

$$\begin{aligned} \text{with } \Lambda &= \text{diag}[\lambda] ; \lambda \in \mathbb{R}^n \\ \text{and } VV^H &= I ; V \in \mathbb{C}^{n \times n} \\ \Sigma &= V\Lambda V^H. \end{aligned} \quad (4)$$

The model may be fitted either to the complex sample covariance matrix [10], [11] or its normalized form, the complex correlation matrix [12].

Both PTA and EVD provide single dyadic approximations of the SCM. Comparing (2) to (3), it is clear that in PTA, the rank-1 dyad ($\psi\psi^H$) merely approximates I_Ω . The systematic phase signature may be fairly assumed to be low rank, or even rank-1 in the absence of multiple systematic signatures in the Ω neighborhood. In the case of EVD, the dyad attempts to explain both the observed interferometric phase (I_Ω) as well as the decorrelation process (Γ). However, the latter is not of a low-rank nature. It may even resemble a symmetric Toeplitz matrix and therefore require the entire spectral components to be sufficiently explained (e.g., in the case of exponential decorrelation). The power of EVD lies in the tomographic separation of the scattering mechanism, where it is separable with respect to the Rayleigh resolution [11]. For the mere purpose of PL, PTA outperforms EVD [1], [18], [19].

In short, PTA provides high estimation efficiency, although at the cost of computational complexity, while EVD is advantageous in terms of computational efficiency but compromises the optimality in phase estimation. Our proposal for efficient PL is a bridge between the two PLs. Similar to the PTA, EMI is an MLE for phase estimation; identical to EVD, it uses eigendecomposition as its solver. EMI is elaborated in Section II-B.

B. EMI as a New Efficient Approach for PL

Let us commence the introduction of EMI from a probabilistic view toward the estimation of SCM [15]. Recalling Σ as a model for the underlying covariance of an n -variate CCG process, the pdf of SCM evaluated from an ensemble of size l follows the complex Wishart distribution [24]:

$$p(C|\Sigma) = c \det(C)^{l-n} \det(\Sigma)^{-l} \exp(-\text{tr}[l\Sigma^{-1}C]) \quad (5)$$

where $\det(\cdot)$ and $\text{tr}(\cdot)$ indicate the determinant and trace operator and c is a coefficient as a function of n and l .

PL may be reformulated into the estimation of Σ via the maximization of the Wishart likelihood distribution [15]. This reformulation is employed hereafter.

We propose the following covariance model for EMI:

$$\begin{aligned} \text{with } \Gamma &\in \mathbb{R}^{n \times n} \\ \alpha &\in \mathbb{R}^{1 \times 1} \\ \text{and } \Xi &= \alpha \text{ diag}[\xi] = \alpha \text{ diag}[\sigma_i \psi_i] \\ \Sigma &= \Xi\Gamma\Xi^H. \end{aligned} \quad (6)$$

The factorization is similar to (3) with the difference that, here, the covariance is approximated by *two* dyads, a full-rank real matrix, and a scaling parameter, i.e.,

$$\Sigma = \alpha^2 \Gamma \circ \sigma\sigma^T \circ \psi\psi^H. \quad (7)$$

This proposal is a slight generalization of the employed factorization of PTA in (3). Similar to PTA, the full-rank matrix is assumed to be known as $\hat{\Gamma}_{ik} = |C_{ik}|$, and the dyadic $\psi\psi^H$ approximates I_Ω and provides the estimated interferograms. Different to PTA, here, the real-valued dyadic $\alpha^2 \sigma\sigma^T$ allows extra freedom for the calibration of $\hat{\Gamma}$, which is expected to be poorly estimated. The introduction of the calibration dyad serves a purpose when the estimation of coherence matrix is erroneous. In the absence of coherence estimation error, calibration is redundant, i.e., $\alpha^2 = 1$ and $\sigma = \bar{1}$.

The MLE of the proposed factorized covariance matrix follows from the maximization of the Wishart pdf given by (5):

$$\begin{aligned}\hat{\Sigma} &= \operatorname{argmax}_\Sigma \{ \ln(p(C|\Sigma)) \} \\ &= \operatorname{argmin}_\Sigma \{ \operatorname{tr}(\Sigma^{-1} C) + \ln(\det(\Sigma)) \} \\ &= \operatorname{argmin}_\Sigma \{ \operatorname{tr}(\Xi^{-H} \Gamma^{-1} \Xi^{-1} C) + \ln(\det(\Xi \Gamma \Xi^H)) \}. \quad (8)\end{aligned}$$

Given that $\hat{\Gamma}_{ik} = |C_{ik}|$, the optimization simplifies to

$$\begin{aligned}\text{with } \xi_i &= \xi_i^{-1} = \sigma_i^{-1} \exp(-j\phi_i) \\ \hat{\Sigma} &= \operatorname{argmin}_{\phi, \sigma, \alpha} \left\{ \alpha^{-2} \xi^H (\hat{\Gamma}^{-1} \circ C) \xi + \ln \left(\prod_{i=1}^n (\alpha \sigma_i)^2 \right) \right\} \quad (9) \\ &= \operatorname{argmin}_{\phi, \sigma, \alpha} \left\{ \alpha^{-2} \xi^H (\hat{\Gamma}^{-1} \circ C) \xi - \sum_{i=1}^n \ln((\alpha \sigma_i)^{-2}) \right\} \quad (10)\end{aligned}$$

Note that ξ is introduced for brevity of notation and is defined as the reciprocal of the elements of ξ .

The above-mentioned double objective optimization is analytically solved via the provided solution in Appendix A, however, at the cost of increased computation. Hereafter, the aim is to substitute this optimization with a proxy, which allows a computationally efficient solution while retaining the estimation efficiency. The sought proxy is defined by the following two steps.

Firstly, the second objective of the formulated MLE is substituted by a linear surrogate to accelerate the convergence of the target optimization. We allow this linearization by the substitution of $\ln(\alpha \sigma_i)^{-2}$ with its first-order Taylor series at the proximity of $(\alpha \sigma_i)^{-2} \approx 1$

$$\hat{\Sigma} = \operatorname{argmin}_{\alpha, \phi, \sigma} \left\{ \alpha^{-2} \xi^H (\hat{\Gamma}^{-1} \circ C) \xi - \sum_{i=1}^n (\alpha \sigma_i)^{-2} + n \right\}. \quad (11)$$

Following this linearization, the second objective is approximated by the norm of the calibration vector.

In the second step toward finding an efficient solver, without loss of generality, the norm of the vector $\sigma^{\circ-1}$ is constrained to \sqrt{n} . Note that the norm of the calibration vector $\alpha\sigma$ is a target of optimization in the second objective term of (11). Therefore, the α parameter adjusts the norm of $\sigma^{\circ-1}$, and the equality constraint can be set to any arbitrary constant.

Addition of the equality constraint is realized through the method of Lagrange multipliers. Aggregating the norm constraint, i.e., $\sum_{i=1}^n \sigma_i^{-2} = \xi^H \xi = n$, the following Lagrangian

results:

$$\hat{\Sigma} = \operatorname{argmin}_{\phi, \sigma, \alpha, \lambda} \{ \alpha^{-2} \xi^H (\hat{\Gamma}^{-1} \circ C) \xi - \dots \alpha^{-2} \xi^H \xi - \tilde{\lambda}(\xi^H \xi - n) \}. \quad (12)$$

Seeking the minimum of (12) through its gradient with respect to ξ yields

$$(\hat{\Gamma}^{-1} \circ C) \hat{\xi} = \lambda \hat{\xi} \quad (13)$$

with

$$\lambda = \alpha^2 \tilde{\lambda} + 1. \quad (14)$$

This is the formulation of eigendecomposition of the Hadamard product $\hat{\Gamma}^{-1} \circ C$, with λ as the *minimum* eigenvalue and $\hat{\xi}$ as its corresponding eigenvector. Appendix B highlights the properties of the Hadamard product.

The last open question concerns the optimum α parameter. In seeking this parameter, let the rearrangement of (13) by the multiplication of $\hat{\xi}^H$ to its left- and right-hand side and further simplification with the considered norm constraint

$$\hat{\xi}^H (\hat{\Gamma}^{-1} \circ C) \hat{\xi} = \lambda n. \quad (15)$$

Substituting (15) into (10) further yields

$$\hat{\alpha} = \operatorname{argmin}_{\alpha, \lambda} \left\{ n \alpha^{-2} \lambda - n \ln(\alpha^{-2}) - \sum_{i=1}^n \ln(\hat{\sigma}_i^{-2}) \right\}. \quad (16)$$

The estimate of α follows from the gradient of the above-mentioned optimization objective with respect to this parameter

$$\begin{aligned}-2n\lambda\alpha^{-3} + 2n\alpha^{-1} &= 0 \\ \hat{\alpha} &= \sqrt{\lambda}. \quad (17)\end{aligned}$$

In summary, considering $\hat{\xi}_i = \hat{\xi}_i^{-1}$, the solution of the Lagrangian as the minimum eigenpair of the Hadamard product $\hat{\Gamma}^{-1} \circ C$ provides the following.

- 1) *Estimated Phase Series:* $\hat{\phi} = \angle \hat{\xi}$.
- 2) *Estimated SCM:* $\hat{\Sigma} = \lambda \hat{\Gamma} \circ \hat{\xi} \hat{\xi}^H$.
- 3) *Estimation Quality Measure:* λ (elaborated in the following).

Note that the same as other PL approaches, the estimation of absolute phase series is ambiguous. The phase of an arbitrary image in the time series is set to zero, and the remaining phases are measured relative to this arbitrary datum. A second caution is in order in setting the norm of the estimated $\hat{\xi}$ value. The eigenvector and the sought solution of Lagrangian belong to the same equivalence class. They merely differ in their norm. EMI requires the vector norm to be \sqrt{n} . To consider this constraint, the eigenvector's norm ought to be adjusted to yield the sought solution of the target Lagrangian by allowing $\hat{\xi} \leftarrow \frac{\sqrt{n}}{\|\hat{\xi}\|} \hat{\xi}$.

Furthermore, λ may be interpreted as a quality measure for the phase estimation, adding a further feature to the proposed estimator. To introduce this measure, let the expansion of (15)

$$\lambda = \frac{1}{n} \sum_{i=1}^n \sum_{k=1}^n \hat{\sigma}_i^{-1} \hat{\sigma}_k^{-1} (\hat{\Gamma}^{-1} \circ \Gamma)_{ik} \cos(\Delta\phi_{ik} - \hat{\phi}_k + \hat{\phi}_i). \quad (18)$$

TABLE I

SUMMARY OF THE PL APPROACHES. ALL APPROACHES ARE ITERATIVE AND THEORETICALLY COMPARABLE IN TERMS OF COMPUTATIONAL EFFICIENCY. REGULARIZATION IS PERFORMED OCCASIONALLY, IN CASES WHERE $\hat{\Gamma}$ IS NOT POSITIVE DEFINITE. IT IMPOSES NEGIGIBLE COMPUTATIONAL BURDEN (SEE SECTION IV-B). REFER TO THE TEXT FOR THE DETAILS ON THE INITIALIZATION AND REGULARIZATION

PL Estimator	SCM Model	Solution	Computation	Exempt of Initialization	Exempt of Regularization	Estimation Efficiency	Coherence Calibration
PTA	$\Sigma = \hat{\Gamma} \circ \psi \psi^H$	Iterative Solution Equation 22	Iterative	✗	✗	✓	✗
EVD	$\Sigma = \lambda v v^H$	Maximum eigen-pair of C	Iterative	✓	✓	✗	✗
EMI	$\Sigma = \alpha^2 \hat{\Gamma} \circ \sigma \sigma^T \circ \psi \psi^H$	Minimum eigen-pair of $\hat{\Gamma}^{-1} \circ C$	Iterative	✓	✗	✓	✓ considered but restricted

Following this reformulation, the Lagrange parameter is seen to reflect the goodness-of-fit of the proposed SCM model of (6) to the data set. Ideally, if $\hat{\Gamma}$ is an adequate estimator of the true statistics of the data, the calibration vector is redundant, i.e., $\sigma = \vec{1}$, and the misfit between the observed and estimated phases is close to zero [see Fig. 1(a) and (b)]. Therefore, following the quasi-bistochastic property of the Hadamard product $\Gamma^{-1} \circ \Gamma$ in Appendix B, the Lagrange parameter yields:

$$\lambda_{\text{ideal}} = \frac{1}{n} \sum_{i=1}^n \sum_{k=1}^n (\hat{\Gamma}^{-1} \circ \Gamma)_{ik} \cos(\theta) = 1. \quad (19)$$

Deviation of λ from 1 indicates the inefficiency of the proposed model in coherence calibration and/or phase estimation. EMI assumes the inadequacy of coherence estimation and increases its model complexity to account for coherence calibration. However, it first limits the calibration to a rank-1 dyadic and second employs a linear approximation. This marginal increase in the model complexity may not be sufficient for efficient calibration of the coherence. The λ parameter provides a measure to indicate EMI's model inadequacy.

C. EMI Versus PTA and EVD

In the decision for choosing the optimum estimator for efficient NRT time series analysis, here, the three estimators are theoretically compared in terms of their computational and estimation efficiency. Table I summarizes this comparison.

1) *Estimation Efficiency*: EMI and PTA follow the MLE in phase estimation with different implicit assumptions. Under the validity of their underlying assumptions, the two estimators are the closest to the CRLB. It is therefore theoretically clear that the two estimators outperform EVD in terms of estimation efficiency (cf., simulation analysis and real data experiments for the quantification of this comparison). Hereafter, the focus is on the mathematical comparison between PTA and EMI.

The difference between the two estimators lies on the introduced degree of freedom by the calibration dyadic [cf., (6) with (3)]. To convey their similarity, let us consider the case of $\lambda = \alpha^2 = 1$ and revisit (11). Substituting the PTA-proposed vector of $\xi = \psi = \vec{1} \exp(j\phi)$ in (11) yields

$$\hat{\Sigma} = \operatorname{argmin}_{\psi} \{ \psi^{\circ-H} (\hat{\Gamma}^{-1} \circ C) \psi^{\circ-1} - \psi^{\circ-H} \psi^{\circ-1} + n \}. \quad (20)$$

Following the gradient of the above-mentioned objective function with respect to ψ gives:

$$(\hat{\Gamma}^{-1} \circ \Gamma \circ I_{\Omega} - I) \exp(j\hat{\phi}) = \vec{0} \quad (21)$$

where I is the identity matrix. Expanding the left-hand side of (21) and rearranging the outcome result in the analytical solution for the sought optimization

$$\exp(j\hat{\phi}_i) = \frac{1}{1 - (\hat{\Gamma}^{-1})_{ii}} \sum_{\substack{k=1 \\ k \neq i}}^n (\hat{\Gamma}^{-1} \circ \Gamma)_{ik} \exp(j(\Delta\phi_{ik} + \hat{\phi}_k)) \quad (22)$$

which is the very iterative solution to the PTA proposed in [8]. PTA imposes the strict model of $\sigma = \vec{1}$. EMI attempts to relax the choice of σ . However, the adaptability of the latter vector is still limited by the employed first-order approximation.

In the absence of coherence estimation error, the two estimators are expected to perform identically, and their parameters are expected to converge ($\lambda \rightarrow 1$ and $\hat{\sigma} \rightarrow \vec{1}$).

2) *Computational Efficiency*: PTA, EVD, and EMI are theoretically comparable in terms of computational efficiency. The latter two estimators resort to eigendecomposition for their solution, while PTA is iteratively solved via (22). The eigendecomposition is as well an iterative approach for finding the eigenpairs. Thus, in terms of computational efficiency, all three estimators are subject to iterative numerical search of the parameter space and expected to have comparable computational complexity. In this regard, the mere computational advantage of EMI and EVD over PTA is the availability of an arsenal of optimized numerical recipes for their efficient solution [25]. However, subject to additional effort and research, the computational efficiency of PTA may be optimized as well.

A note is in order for a thorough analysis of the computational efficiency of PTA. In [9], the expensive Broyden–Fletcher–Goldfarb–Shanno algorithm is suggested for solving the corresponding optimization of PTA. A more efficient approach is suggested in [8] via the iterative solution of (22). However, the latter requires an initialization step. As conveyed in the continuation of this paper, both the convergence speed of the iterative optimization and its estimation efficiency are influenced by the choice of initialization. Guarneri and Tebaldini [8] introduce the “phase of the vector minimizing the quadratic form $\{\psi^H \hat{\Gamma}^{-1} \circ C \psi\}$ ” as their choice of initialization. We interpret this *minimizing vector*

as the *minimum* eigenvector of the Hadamard product $\Gamma^{-1} \circ C$ (which is the solution of EMI). According to our simulation studies and real data experiments, this initialization enhances the convergence speed of the PTA. Moreover, it occasionally improves the performance of phase estimation. Therefore, we favor this initialization for the iterative PTA, as it affects both the estimation and computational efficiency. Adopting this initialization, PTA must not only afford for the same eigendecomposition employed by EMI but also shall undergo an iterative search for fitting the ψ model to the data. Thus, compared with EMI, it imposes an additional computational burden on PL. The extra cost is not justified by any gain in the estimation efficiency (see Sections III-A and IV-A). If initialized differently, the number of iterations for PTA to converge increases, further compromising the computational efficiency (see Section IV-B).

Another note concerns the additional matrix inversion operation in evaluating $\hat{\Gamma}^{-1}$, as required by EMI and PTA. In rare cases, where the coherence matrix is not positive definite, a regularization of the matrix is required prior to inversion. Regularization is efficiently performed via gradual increase of small negative eigenvalue(s) of the coherence matrix, as explained in [1] and [17]. Therefore, PTA and EMI undergo an additional matrix inversion plus occasional regularization compared with EVD. These operations marginally increase the computational cost as the price for an improved estimation efficiency. Section IV-B corroborates the negligibility of this additional cost.

In efficient solution of eigendecomposition, one of the most recent numerical recipes is provided by the method of *multiple relatively robust representations* (MRRR) [26]. This numerical approach allows the efficient retrieval of a subset of eigenpairs with reduced complexity compared with retrieving all eigenpairs. For EMI, the minimum eigenpair is merely desired, decreasing the latter complexity.

III. PERFORMANCE ASSESSMENT: SIMULATION STUDY

Using simulations, here, the performance of EMI is validated and compared with the state-of-the-art algorithms.

Reflected in the coherence matrix, the performance of PL algorithms is bound by signal decorrelation [16]. Considering a generic decorrelation model [27]

$$\Gamma_{ik} = (\gamma_0 - \gamma_\infty) \exp(-\delta t_{ik}/\tau) + \gamma_\infty \quad (23)$$

and introducing γ_0 and γ_∞ , respectively, as the short-term decaying and the long-term persistent coherence, δt as the corresponding temporal baseline, and τ as the signal correlation length, two contradicting decorrelation scenarios are introduced for PL. In the first, $\gamma_\infty = 0$, indicating the total decorrelation of the interferometric signal beyond temporal baseline of $\delta t \sim 4\tau$, while in the second, $\gamma_\infty \neq 0$, rendering even the long temporal baseline interferograms to bear a coherent signal. The presence of such, even weak, long-term coherent signal has been shown to have a strong impact on the performance of PL [1], [28]. The first scenario is hereafter referred to as the *exponential decay* and the second as the *long-term coherence*.

For the investigations of this section, two coherence matrices are simulated following the aforementioned scenarios. γ_0 is set to 0.6 in both cases, while γ_∞ is, respectively, 0 and 0.2 for the exponential decay and long-term coherence. Based on the coherence matrices, two stacks of 50 images each containing an ensemble of 300 statistically homogeneous samples are synthesized as follows: a CCG process is assumed in the generation of the data stack; the stationarity of the interferometric signal within the ensemble is imposed by setting the topographic- and atmospheric-induced phase components to zero; the deformation phase is simulated with a temporal linear trend with a velocity of 1 mm/year; and the temporal sampling interval, similar to Sentinel-1, is set to six days. τ is set to 50 days.

A. Performance in Phase Estimation

As highlighted in [1], [18], and [19], the performance of PTA is affected by the well-known error in the coherence estimation [20], [21]. Recall that PTA uses the inverse of the coherence matrix as the optimum weighting. The high sensitivity of PTA to coherence error is due to the amplification of coherence estimation noise by the inverse operator. Using the same metric for weighting the data, EMI is prone to the same noise amplification by the inverse of the erroneous coherence. In order to investigate this effect, PL is studied in two cases as follows.

- 1) In the first case, $\hat{\Gamma}$ is set to the simulated coherence provided by (23), representing an ideal case where the optimum estimate of the coherence is at hand and the coherence error is negligible.
- 2) In the second case, $\hat{\Gamma}$ is set to the estimated coherence of (1). This case is closer to reality as coherence is unknown and its estimation is inevitable.

The RMSE of phase estimation is reported in Fig. 1(a) and (b) for the former and Fig. 1(c) and (d) for the latter case. The theoretical lower bound for PL is provided by CRLB [16].

As revealed in Fig. 1(a) and (b), in the absence of coherence estimation error, EMI and PTA perform identically and close to the CRLB, while EVD provides a suboptimum estimation deviant from the CRLB. However, the coherence estimation error degrades the performance of the probability-based estimators, as evident from Fig. 1(c) and (d). In Fig. 1(c) and (d), two solutions are considered for the phase estimation, namely the conventional PL processing based on the full data stack and the proposed Sequential Estimator of [1] (ministacks of 10 images and compression to 1 component are considered here). As evident, using EMI as its PL algorithm, the *Sequential Estimator* is able to slightly improve the performance and approach the CRLB. The Sequential Estimator improves the performance thanks to two implicit effects. First, it bounds the analysis to isolated mini-stacks within which the drop of coherence to zero is limited. Second, in the formation of the artificial interferograms between the isolated mini-stacks, an implicit filtering occurs. The latter enhances the efficiency of coherence estimation for the respective artificial interferograms [1].

The degraded performance of PL in the case of exponential decay compared with the long-term coherence is due to the

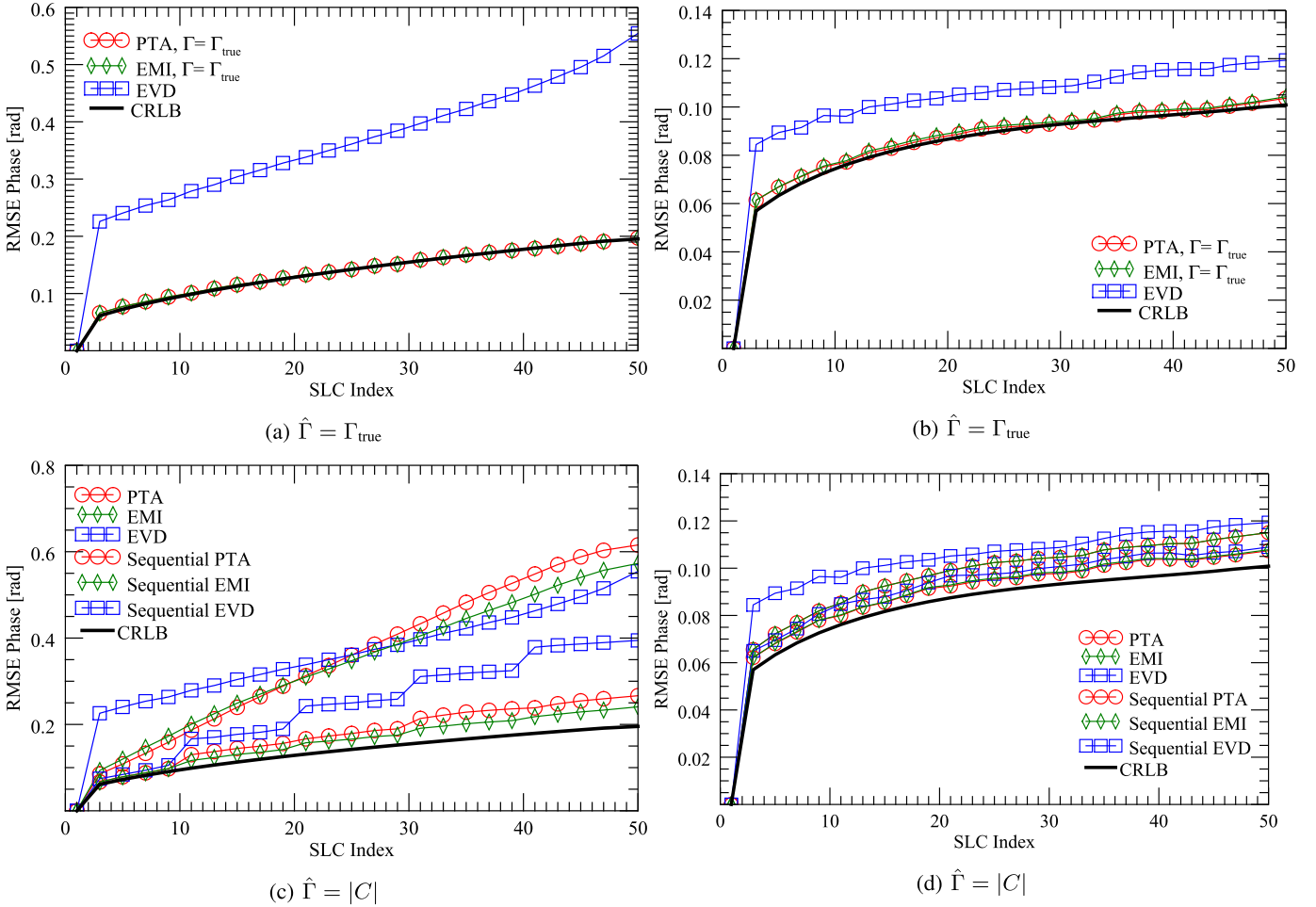


Fig. 1. Performance assessment of different PL estimators compared to CRLB using simulated cases: (a) and (c) exponential-decaying scenario, (b) and (d) long-term coherence. The impact of coherence estimation error on PL is studied in (a) and (b) the absence and (c) and (d) the presence of this error. In (a) (b) and (d), where coherence estimation error is absent/insignificant, EMI performs identical to PTA. In (c), where coherence is significantly erroneous, EMI performs slightly better than the PTA. EVD is shown to be suboptimum in phase estimation, as apparent from (a) and (b) where its performance is highly deviant from the CRLB.

pronounced coherence estimation error for the former. The estimation of coherence degrades significantly for coherence close to zero [20], [21]. In the case of long-term coherence, the presence of low coherent signal prevents the drop of coherence to zero. It is therefore exempted from the significant coherence estimation error for zero coherence.

Note that the error in coherence estimation decreases by the increase in the size of homogeneous ensemble Ω . However, the enlargement of Ω is restricted, as the stationarity of the systematic signals may be violated over large spatial windows. In practice, even if the topography is compensated with high accuracy/precision or is irrelevant, the correlation length of the atmospheric and deformation signal plays a role in violation of stationarity.

B. λ as a Quality Measure

In Section II-B, the Lagrange parameter λ was proposed as a quality measure for phase estimation. The attempt here is on the evaluation of this proposition by comparing λ to a conventional *a posteriori* quality measure. Here, the *a posteriori* coherence of [9] is considered for this purpose,

which reads as

$$\gamma_{\text{apt}} = \frac{2}{n(n-1)} \sum_{i=1}^n \sum_{k=i+1}^n \cos(\Delta\phi_{ik} - \hat{\phi}_k + \hat{\phi}_i) \quad (24)$$

and provides a goodness-of-fit of the estimated phases. Compared with λ in (18), γ_{apt} only reflects the phase misfit, while λ indicates the inadequacy of the stochastic model as well as the residual phase error. To investigate the correlation between the two measures, the same simulation strategy of Section III-A is pursued with a slight change; here, the parameter l , i.e., the size of the ensemble Ω , is varied. As l increases, the coherence estimation asymptotically approaches its optimum performance [20], [21]. As a consequence of the decreased coherence error, a gain in the performance of PL is expected. Theoretically, such gain shall be reflected in both the conventional and proposed quality measures. Fig. 2 corroborates this hypothesis by showing the approach of γ_{apt} and λ to 1 as the coherence estimation improves. It also reveals the correlation between the two quality measures.

Note that the performance of the coherence estimation is known to be degraded for coherence levels close to 0. The

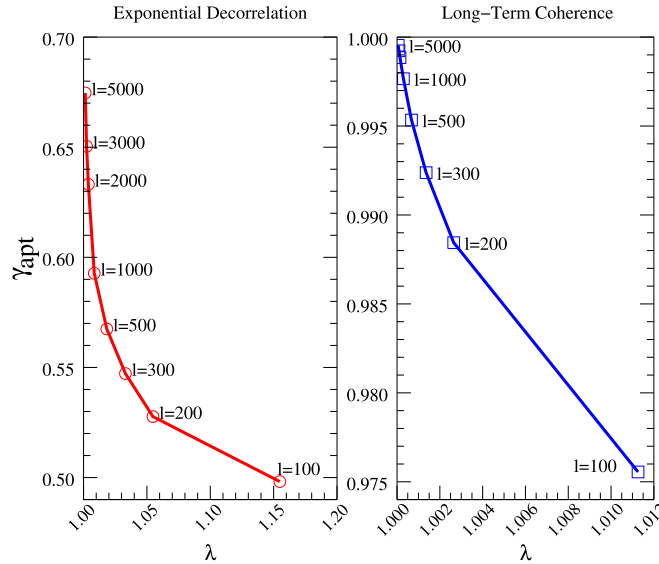


Fig. 2. Correlation between the Lagrange parameter as the proposed quality measure and the *a posteriori* coherence using simulated cases for a varied size of ensemble (l). As l increases, coherence estimation asymptotically approaches its optimal performance and its error decreases, leading to the improvement of phase estimation in PL. The enhanced PL performance is reflected in the approach of both quality measures to 1.

latter is the case in the exponential-decaying scenario. In the long-term coherence, the presence of weak coherent signal, with $\gamma_\infty = 0.2$, prevents the drop of coherence to zero; hence, the improved performance of the coherence and consequently the quality measures.

IV. EXPERIMENT WITH REAL DATA

A time series of Sentinel-1 data over the Italian island of Vulcano is chosen as a test site for the demonstration of EMI. Fig. 3 provides a view of the island from optical and SAR amplitude data, revealing the variety of land cover in the scene. Data in interferometric wide-swath mode and VV polarization are obtained for this test site. The time series is acquired from December 2014 to April 2016 from a descending orbit, providing 38 SLCs. Fig. 4 presents the coherence of the observed interferograms with the shortest and longest temporal baselines, revealing the severe temporal decorrelation of the data set. Fig. 4(c) shows the observed interferogram pertaining to the longest temporal baseline of 564 days. The coherence maps and the observed interferogram are estimated by spatial adaptive multilooking using the Anderson–Darling statistical similarity test on the amplitude data [29]. The aim of PL is to enhance the spatial estimation of the interferograms via the exploitation of the time series.

PL estimates the wrapped phase series, inclusive of the geophysical and atmospheric signals. Isolation of the geophysical signal of interest follows from the second processing step as in the case of PSs [5], [8]. Phase estimation is performed on the full spatial resolution. However, the pointwise complex coherence matrices are estimated based on an ensemble of pixels in the homogeneous Ω region surrounding each pixel. Ω is detected via the Anderson–Darling statistical similarity

test with a false-alarm rate of 5%. Regions with an ensemble size of 100 pixels and larger are detected as DS; only the DS undergoes PL. To improve the spatial stationarity in the homogeneous region, the topographic-induced phase is simulated using the SRTM digital elevation model and subtracted from the SLCs prior to the coherence estimation.

The focus of this experiment is to compare the different PL approaches in terms of estimation and computational efficiency. Therefore, PL is performed via EMI, PTA, and EVD. The PTA is solved efficiently using (22) and initialized with two different strategies as follows.

- 1) *PTA 1*: Using the phase of the minimum eigenvector of $\hat{\Gamma}^{-1} \circ C$, i.e., $\hat{\phi} = \angle \hat{\xi}$.
- 2) *PTA 2*: Using a null vector of $\hat{\phi} = \vec{0}$.

Therefore, four different cases are compared in total. The implementation details of all compared cases are kept similar as far as the estimators allow.

A. Performance Assessment in Phase Estimation

EMI's performance is assessed and compared with different approaches from four aspects.

1) *Visual Inspection*: The performance of PL in phase estimation may be visually assessed from the inspection of the estimated interferograms. The longer temporal baseline interferograms are expected to undergo a more severe temporal decorrelation. Therefore, the inspection of such interferograms is more conclusive for the examination of the merit of the performed temporal phase filtering by PL. Bearing this in mind, the largest temporal baseline interferogram with a baseline of 564 days is chosen to be presented in Fig. 6. Comparison of these interferograms to the observed interferogram of Fig. 4(c) reveals the improved phase estimation achieved by PL. Furthermore, the performance of EMI may be compared with PTA estimated interferograms. The difference in their performance is specifically visible over the volcanic caldera (indicated by boxes). Note that the improved performance of EMI over PTA approaches, as well as the role of different initializations in the performance of PTA, by inspecting the spatial noise of the estimated interferograms over the caldera.

Due to the visual similarity of EVD and EMI estimated interferograms, their difference is provided instead (see Fig. 5). Similar to EMI, EVD is successful in recovering the signal over the caldera.

2) *A Posteriori Coherence*: The estimation quality of EMI, PTA1, and PTA2 is further assessed in Fig. 7 via the provision of the *a posteriori* coherence of (24). Inspecting the quality of EMI shows a reasonable performance in phase estimation, except for the sparse vegetated areas and the surrounding water. Note, for instance, that the volcanic caldera, as one of the geophysically interesting parts of this test site, is retrieved with the coherence of ≥ 0.9 .

Comparing these three estimators specifically over the volcanic caldera, the inferred improved performance of EMI over PTA, as well as PTA1 over PTA2, is confirmed. Investigating the behavior of PTA over the low-quality part of the volcanic caldera reveals its failure in convergence to a solution for 40% of cases (convergence criterion is defined as phase estimation



Fig. 3. View of the Vulcano Island located in Southern Italy. (Left) Optical image from Google Earth showing the various land cover of the chosen test site. (Right) Temporally averaged amplitude map of the test site estimated from 38 SLCs of the Sentinel-1 SAR data stack.

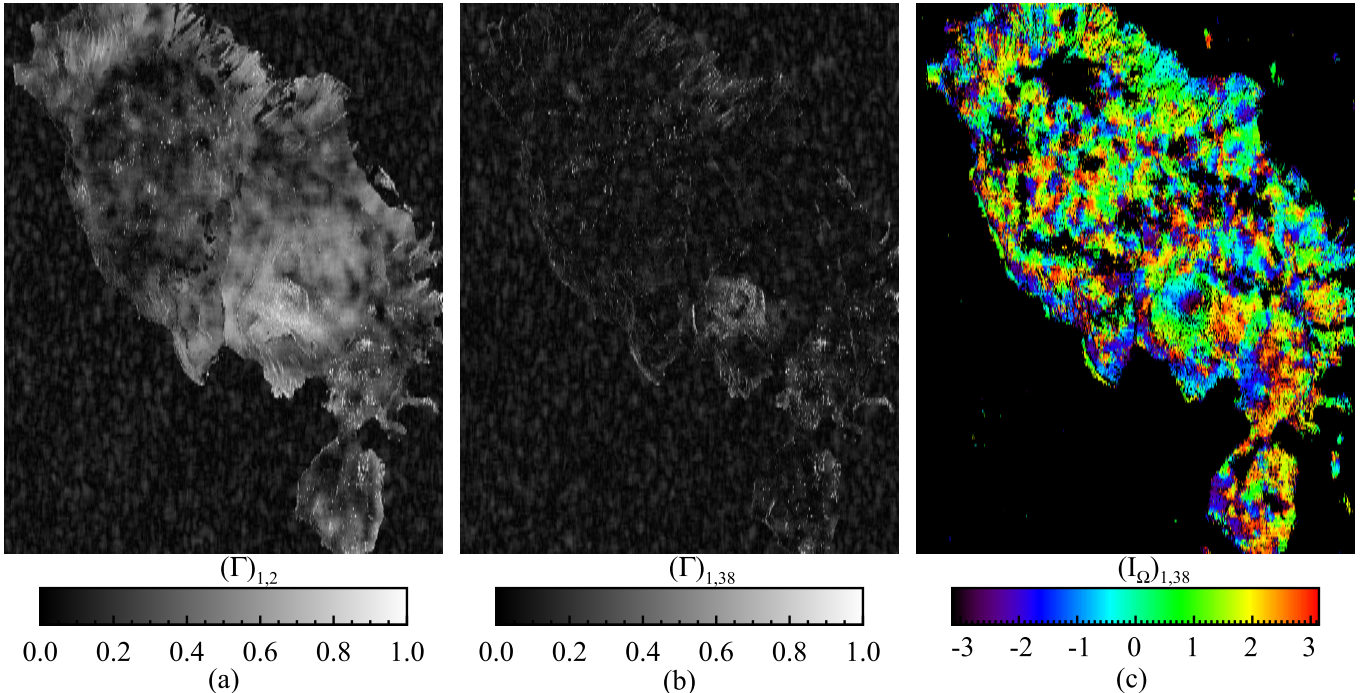


Fig. 4. Interferometric data of Vulcano; coherence of the observed interferograms with temporal baseline of (a) 12 and (b) 564 days, and (c) observed interferogram of the latter. These maps are estimated by spatial adaptive multilooking. Comparing the coherence map of the shortest and longest temporal baseline interferograms in (a) and (b) indicates the severity of the temporal decorrelation. The goal of PL is to improve this spatial estimation of interferograms via the exploitation of the time series (see Fig. 6 for visual inspection of the enhancement in interferogram estimation).

with a precision of 10^{-3} rad; the maximum permissible number of iterations in the parameter search is set to 4000 iterations). In Appendix C, a simulation analysis over this area is reported.

3) Quantitative Assessment—Cross Comparison of the Estimators: Here, the focus is on the quantification of the difference between the three estimators. Setting EMI as the benchmark for this analysis, the discrepancy between the

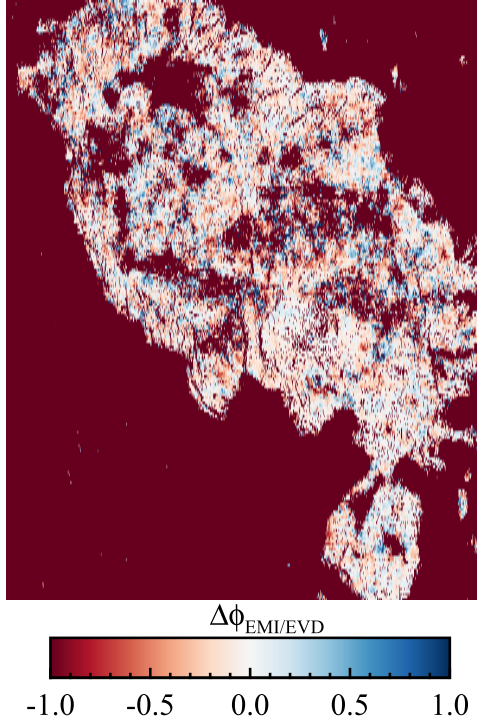


Fig. 5. Spatial inspection of the difference in interferogram estimation (temporal baseline: 564 days), employing EMI and EVD.

estimated phases of PTA1 and EVD with the latter is evaluated for each resolution cell in the time series. Having performed PL in a pixelwise fashion, the phase discrepancies consist of $r_{rg} \times r_{az}$ values in the spatial direction and $n - 1$ values in the temporal direction. To have a statistical analysis on the performance, the $r_{rg} \times r_{az} \times (n - 1)$ values are accumulated. The spatio-temporally accumulated phase discrepancies are clustered according to their respective *a posteriori* coherence. The normalized histogram of each cluster is presented, with its first- and second-order moment describing the bias and variance of each estimator with respect to EMI, respectively. The resulted normalized histograms are presented in Fig. 8. Note that the quantitative assessment is relative to EMI. An independent assessment follows in Section IV-A4 to answer the question on which PL outperforms the others.

In analyzing Fig. 8(a), the bias and variance of EMI compared with PTA decrease as the *a posteriori* coherence increases, as theoretically expected. Coherence level of $\gamma_{apt} \geq 0.6$ is associated with cases where $\hat{\Gamma}$ is an efficient estimator of the coherence (see Section III-A). In such cases, the calibration dyadic is expected to be redundant, and the performance of EMI and PTA in phase estimation is expected to be similar. EMI's model diverges from PTA for lower coherence levels, explaining the increase in the variance between the two. However, it is important to notice that the two estimators are unbiased with respect to each other, even at low coherence levels. Comparing Fig. 8(a) and (b), the theoretical degraded estimation efficiency of EVD compared with the probabilistic-based approaches is verified. Note that the increased bias and variance of EVD are compared with EMI at different

coherence levels. The latter observation justifies the selection of EMI compared with the EVD.

4) Quantitative Assessment—Variation in SNR: The discrepancy between the estimators has been cross compared in Section IV-A3. The focus in this section is on the *independent* performance assessment of PL approaches. Recall that PL is devised for improving the SNR of the spatially multilooked interferograms in I_Ω . Therefore, we propose the variation in SNR of the estimated interferograms relative to I_Ω as a potential-independent quality measure

$$\delta\text{SNR} = \text{SNR}_{\hat{\phi}} - \text{SNR}_\phi = 10 \log_{10} \left(\frac{\delta_\phi^2}{\delta_{\hat{\phi}}^2} \right) \quad (25)$$

where δ^2 represents the phase variance and its subscripts $\hat{\phi}$ and ϕ indicate the PL-estimated versus the spatial-multilooked interferograms. The variance δ^2 is estimated spatially for each interferogram in a pixelwise fashion as follows: a symmetric window is considered about each pixel (200 m in the range/azimuth direction). The ensemble of phases falling in this window is used for variance estimation. Note that the employed coarse ensemble selection criterion does not guarantee the stationarity of the interferometric signal within the estimation window. To account for the arising heterogeneity, the variance shall be estimated robustly to withstand the outlying samples [30]. Among different robust estimators of variance [31], the normalized median absolute deviation (MAD) is chosen here [32], [33]. MAD has a high breakdown point of 50%, i.e., it resists 50% contamination of the ensemble by outliers. It reads as [32]

$$\hat{\delta}_{\text{mad}} = 1.4826 \text{ median}(|\phi - \text{median}(\phi)|) \quad (26)$$

where ϕ represents the ensemble. The normalization constant 1.4826 renders the estimator consistent with the standard deviation of a normal distribution. In the presence of high-frequency systematic signal within the assumed 200-m distance, MAD is expected to resist against the nonstationarity up to its breakdown point. However, it fails in noise estimation beyond this tolerance.

Note that in the evaluation of δSNR for each estimator, the low-quality result pertaining to $\gamma_{apt} \leq 0.35$ is excluded. In the case of PTA1, the failed estimation result over the caldera is disregarded by this masking. The surrounding water of the island is as well masked by this thresholding.

For a concise quantitative analysis over the entire spatio-temporal extent of the data, the estimated δSNR values are aggregated spatially over each interferogram in the time series. The median of such aggregated data provides a robust measure for the overall performance of PL for each interferogram. Fig. 9 reports the barplots of overall δSNR for each interferogram as a function of their temporal baseline. EMI, EVD, and PTA1 are compared in Fig. 9. As apparent, EMI slightly outperforms the other approaches throughout the time series. A feature worthy of notice is the exacerbated noise of the estimated interferograms with temporal baseline of 12 and 24 days. In the mentioned interferograms, the performance degradation of EMI and EVD is the least and most pronounced, respectively.

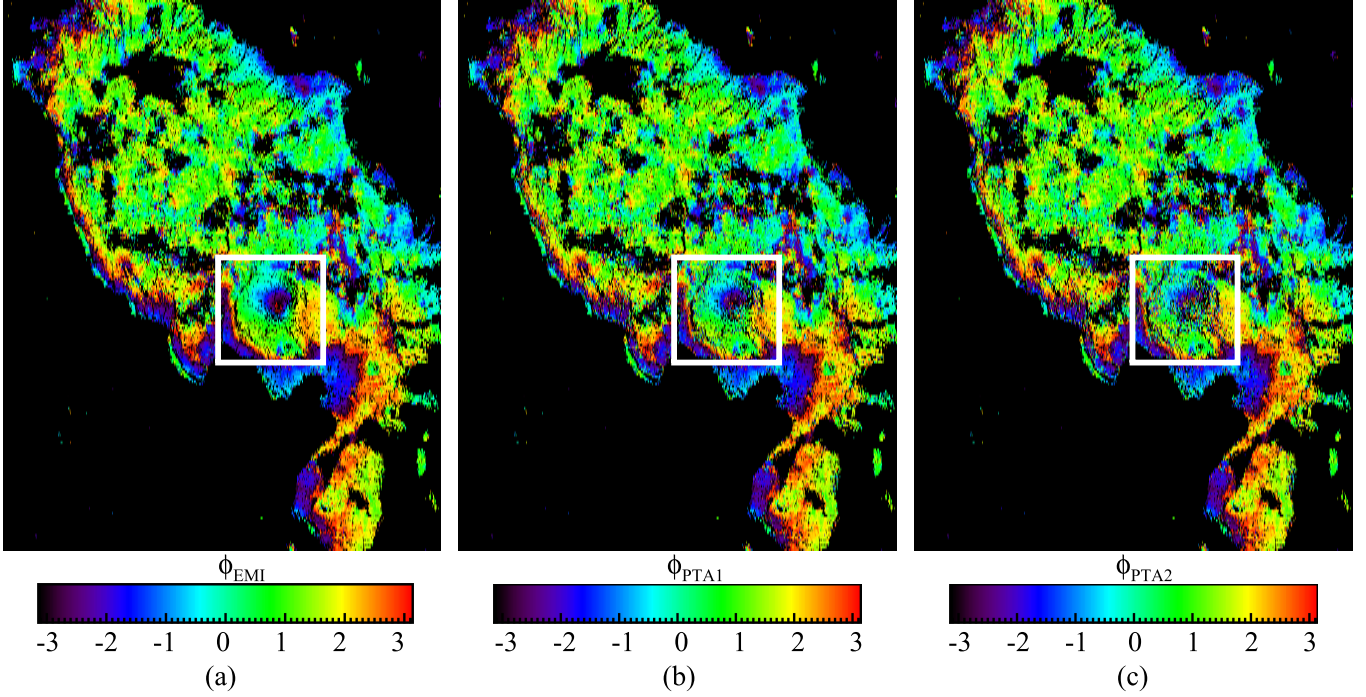


Fig. 6. Spatial inspection of the estimated interferograms with the longest temporal baseline of 564 days: the estimated interferogram using (a) EMI, (b) PTA1 initialized by the solution of EMI, and (c) PTA2 initialized by null phases. Compared with EMI, the performance of PTA estimators is seen to be degraded over the volcanic caldera, indicated by the box. Note also that the different initialization is seen to impact the estimation efficiency over the caldera. Appendix V reports on a simulation analysis based on the volcanic caldera.

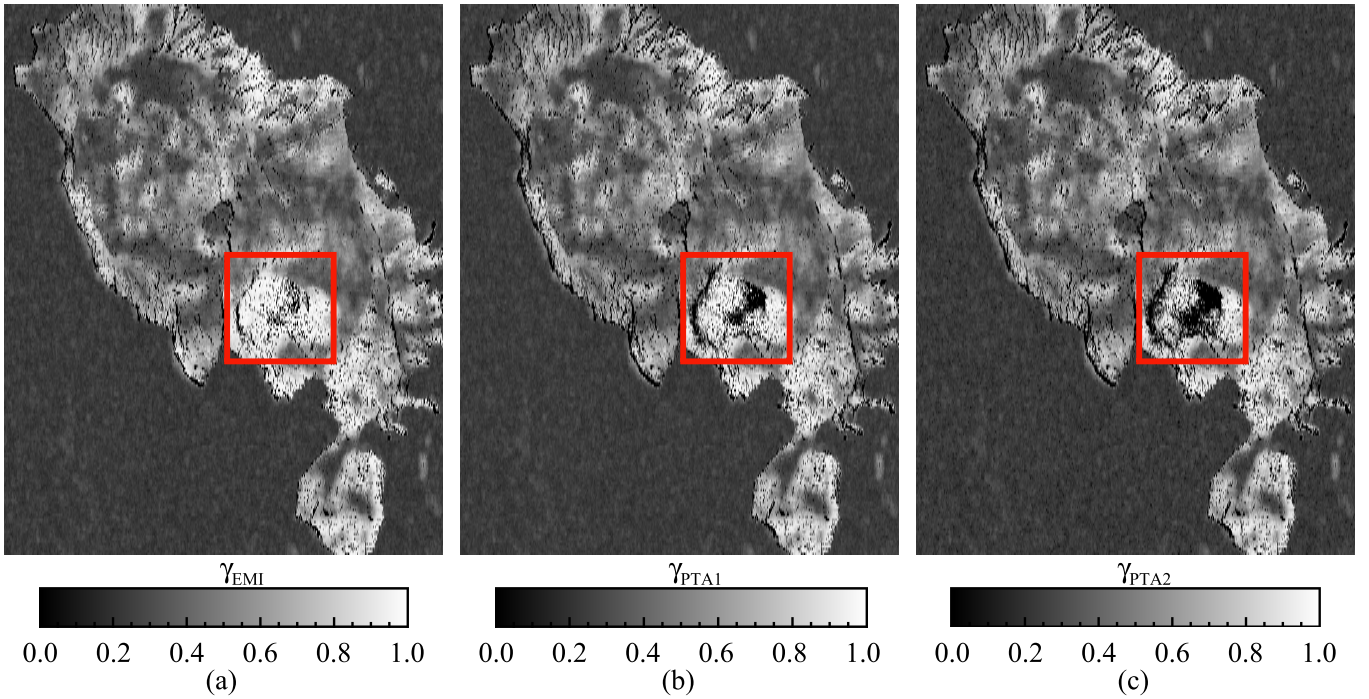


Fig. 7. *A posteriori* coherence as the quality measure for phase estimation performed by (a) EMI, (b) PTA1 initialized by the solution of EMI, and (c) PTA2 initialized by null phases. Note that the degraded quality of PTA estimators in comparison with EMI over the volcanic caldera. The figures verify the conclusions about estimation efficiency inferred from Fig. 6.

This independent evaluation of the estimation efficiency proves the optimality of EMI over EVD and PTA and therefore validates the choice of EMI as a benchmark for comparisons of Section IV-A3 and the reported estimation bias and efficiency therein.

5) *Summary:* The following conclusions are drawn from the performed comparisons.

- 1) The result over the volcanic caldera proves the improved efficiency of EMI compared with PTA in terms of phase estimation (see Figs. 6 and 7).

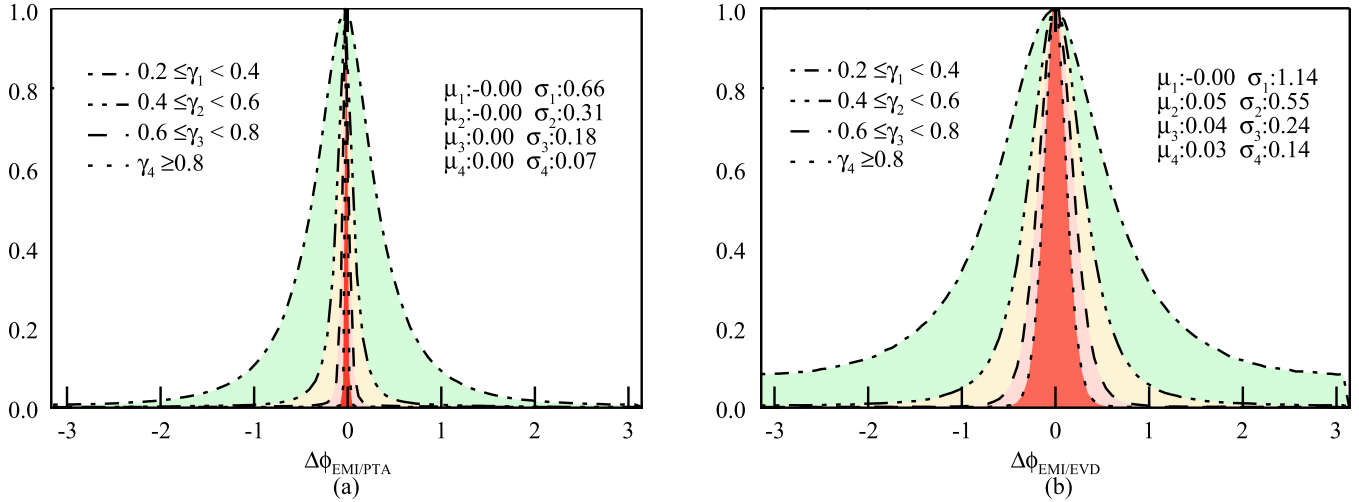


Fig. 8. Spatio-temporal assessment of the estimation bias and variance compared with EMI at different *a posteriori* coherence levels as a quantitative assessment of phase discrepancy between EMI and (a) PTA1 and (b) EVD. The bias (μ_i) and standard deviation (σ_i) of the estimators are reported relative to the *a posteriori* coherence, with i referring to the reported coherence level. The agreement between the methods increases with the increase of the coherence. This analysis is relative to EMI, an independent quantitative assessment follows to validate EMI as an outperforming estimator.

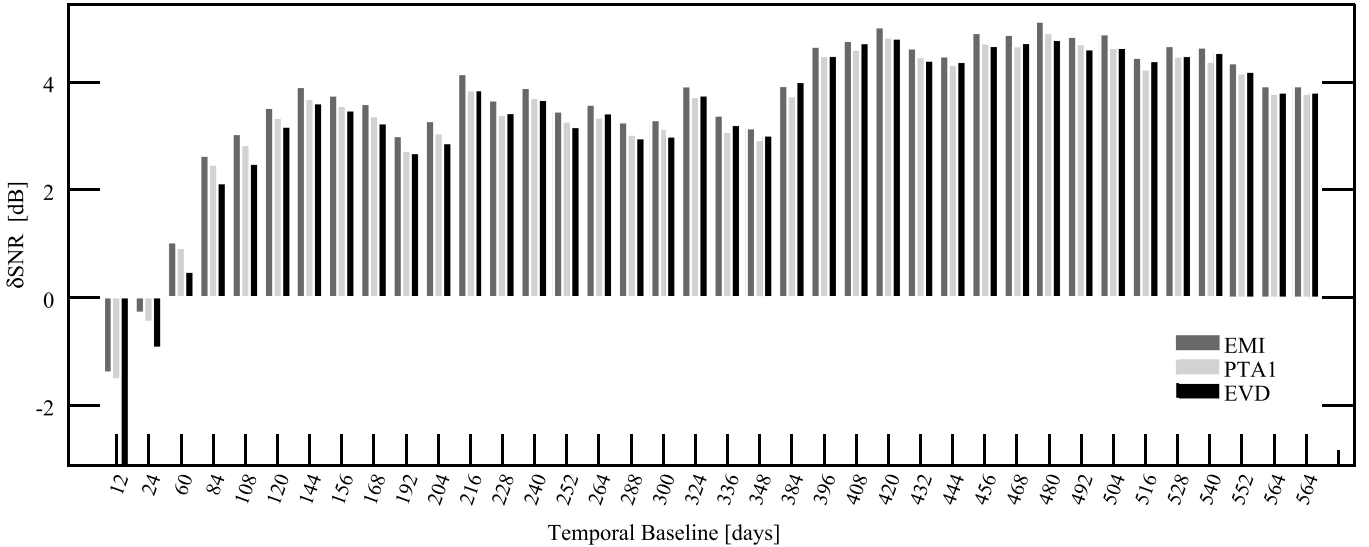


Fig. 9. Temporal assessment of δSNR , as an independent quality descriptor of each PL approach; reported for the time series of estimated interferograms. Positive values of δSNR indicate improved SNR of the PL-estimated over the spatially multilooked interferograms. As an overall trend, EMI is observed to slightly outperform EVD and PTA. This behavior is in line with the conclusions of the simulation analysis in Fig. 1(c) and (d).

- 2) The initialization of PTA is proved to have an impact on its estimation efficiency (see Figs. 6 and 7)
- 3) Between the two compared initialization methods, the eigenvector is a more efficient approach (see Figs. 6 and 7).
- 4) PTA's subjective choice of initialization highlights the merit of EMI in efficient data processing, as the latter is exempt from initialization.
- 5) PTA1 is initialized by the solution of EMI and spends extra effort on fitting its model through further iterations. The additional iterative solution not only imposes extra computation but may also compromise the estimation efficiency and cause divergence from an optimum solution (see Figs. 6 and 7).
- 6) EVD is quantitatively shown to increase the estimation

bias and variance compared with the probabilistic-based approaches (see Figs. 8 and 9).

- 7) The negligible increment in the computational cost of EMI with respect to EVD increases the estimation efficiency (see Figs. 8 and 9).

B. Computational Efficiency

The cumulative processing time of PL for the entire scene is provided in Fig. 10 in order to assess the computational efficiency of different approaches. Note that the reported run time excludes the preprocessing/postprocessing steps of PL (e.g., adaptive multilooking). To insure the validity of these comparisons, the implementation of the estimators is kept similar, as far as the algorithmic details allow. However, EMI

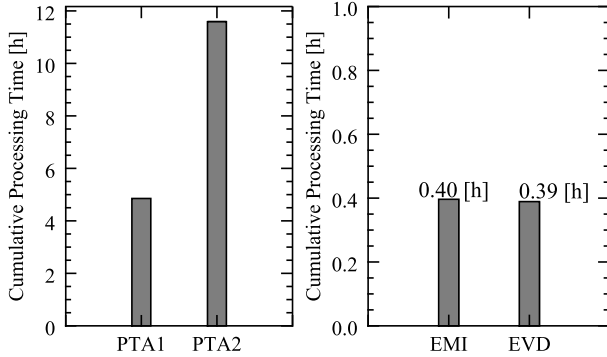


Fig. 10. Cumulative processing time of the estimators over the entire test site as an assessment of computational efficiency. Note that the cross comparison of the left and right plots is inadmissible due to difference in implementation of the estimators. However, the within plot comparisons are fair and conclusive. The comparison of EMI and EVD reveals the negligible imposed computation of the latter. PTA1 and PTA2 differ only in their initialization; their comparison highlights the impact of initialization on the computational efficiency.

and EVD benefit from highly optimized eigendecomposition libraries, namely the MRRR method, while PTA employs a self-developed optimization module based on the analytical solution of (22) proposed in [8]. Due to this reason, the direct comparison of eigendecomposition-based solvers to PTA approaches is unfair and inconclusive. EMI may, however, be fairly compared with EVD and PTA1 with PTA2. From the comparison of EMI to EVD, it is apparent that the additional computation, regarding the coherence matrix inversion and its occasional regularization, has negligible impact on the computational efficiency of EMI. Comparison of PTA1 and PTA2 highlights the impact of initialization on the computational efficiency of PTA. Note that the first initialization method improves the efficiency by $\approx 50\%$.

The convergence behavior of PTA is further investigated, revealing that PTA1 and PTA2 fail in convergence over 7% and 18% of the test site, respectively. According to the spatial analysis, failures in convergence occur over the volcanic caldera as well as the surrounding water. A comparison between the number of iterations of PTA is presented in Fig. 11. For visualization purposes, the axis is limited to 400 iterations, and convergence failures occurring at 4000 iterations are excluded. The plot illustrates that nearly 11% of the scene convergence occurs with less than 10 iterations for PTA1, indicating that the solution of EMI and PTA coincides for the respective regions. Also noticeable is the increase in the number of iterations from PTA1 to PTA2, which is another proof on the impact of initialization.

Spatial analysis of the convergence behavior shows that PTA mostly spends its computational effort over fast decorrelated regions. Examples are the surrounding water as well as the sparse vegetated areas of the island, for which the *a posteriori* quality of phase estimation is poor. Due to their low quality, such regions will be discarded in post-PL steps. This observation proves that the additional effort of PTA for fitting its model is not rewarded by any information gain in terms of improving the spatial sampling.

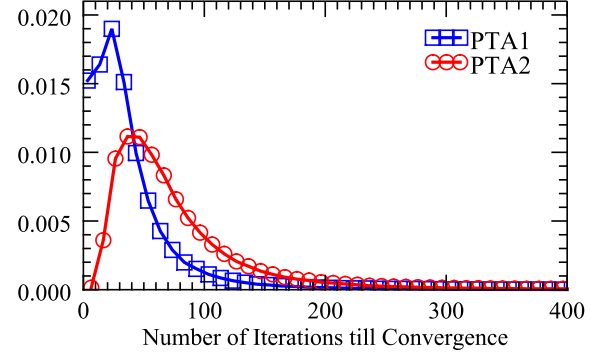


Fig. 11. PDF of the number of iterations performed by PTA. For visualization, the reported iteration range is limited, despite the maximum allowable iteration of 4000. 7% and 18% of the scene fail in convergence after 4000 iterations by PTA1 and PTA2, respectively.

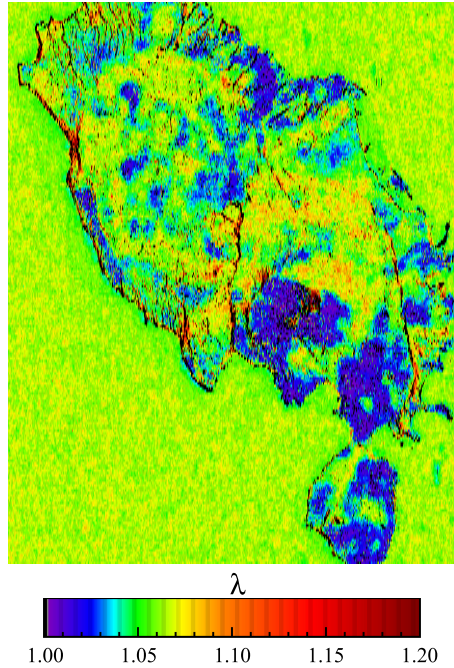


Fig. 12. Lagrange parameter as a by-product of EMI. The closer the parameter is to 1, the better is the fit of the EMI model to the data stack.

Final word on the computational efficiency regards the comparison between EMI and PTA. Recall that the PTA1 is initialized by the solution of EMI. It therefore has the iterative analytical solution as an additional computation step compared with EMI. On average, PTA1 performs 300 iterations for fitting its model. This effort has been shown to be in vain, as it does not improve the estimation efficiency and in part even results in divergence from an optimum phase estimation (e.g., over the caldera in Figs. 6 and 7). Therefore, EMI is argued to be computationally more efficient than PTA.

C. Performance of λ as a Quality Measure

The Lagrange parameter of EMI has been introduced as a quality measure for phase estimation. Fig. 12 reports this parameter for the test site. In order to validate the merit of λ as a quality measure, its relation with the *a posteriori* coherence

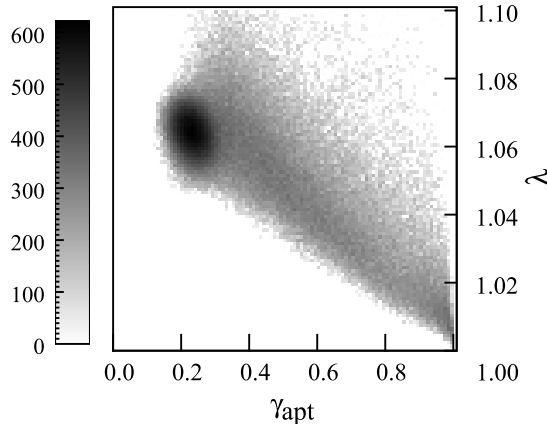


Fig. 13. Bivariate distribution of the two quality measures for all pixels in the scene. The correlation between the Lagrange parameter as a proposed quality measure and the *a posteriori* coherence is observed. The approach of both parameters γ_{apt} and λ to 1 indicates the validity of the EMI model for the DS region. The center of this pdf at $\gamma_{apt} = 0.23$ and $\lambda = 1.065$ pertains to the surrounding water as well as the dense vegetated area over the island (see Fig. 12).

is investigated here. Fig. 13 shows the bivariate distribution of the two measures for all pixels in the scene and reveals a strong correlation between the two. The observed correlation is explained based on the hypothesis of Section II-B; the approach of λ to 1 indicates the goodness-of-fit of the SCM model proposed by EMI as well as the convergence of models in PTA and EMI. The center of this pdf at $\gamma_{apt} = 0.23$ and $\lambda = 1.065$ pertains to the surrounding water as well as the dense vegetated area over the island (see Fig. 12). These areas are masked from the presented interferograms in Fig. 6.

V. CONCLUSION AND DISCUSSION

The coherence estimation error is known to affect the performance of PL in general and PTA in particular. In the current contribution, it has been demonstrated that the error affects the computational efficiency of the algorithm as well. In the interest of improving the estimation and computational efficiency and approaching further to NRT processing of the emerging SAR Big Data, we allowed the generalization of the PTA proposed model. In modeling the SCM, the proposed generalization accounts for the calibration of the (erroneous) coherence matrix by a rank-1 dyad. An MLE of the proposed model has been presented. The reference MLE has been approximated and constrained to arrive at an efficient PL, provided by the method of Lagrange multiplier. Both the eigenvalue and eigenvector of the Lagrangian solution have been investigated as effective parameters for NRT data processing. Via simulation, EMI has been shown to retain estimation efficiency close to the CRLB.

Aside from the proposal of EMI, the efficient implementation of PTA in [8] has been brought into light. The estimation and computational efficiency of the PTA have been shown to be influenced by its initialization choice. This impact asserts the advantage of eigendecomposition-based solvers in PL, as they are exempted from initialization.

The EVD estimator has been argued to be suboptimum in phase estimation. This theoretical proposition has been validated with simulation analysis and real data experiments. The advantage of MLEs over the EVD is especially noticeable with improved coherence estimation [see Fig. 1(a) and (b)]. Upon enhancing coherence estimation, e.g., by *nonlocal* approaches [34], [35], the performance of EMI improves beyond the reported values in real data experiments. Furthermore, the MLE-based approaches have been shown to be the outperforming candidates for efficient time series analysis with Sequential Estimator [1] [see Fig. 1(c)]. The computational efficiency of EMI has been compared with EVD to verify the former as an agile algorithm for NRT processing. Through simulation and real data experiments, EMI was shown to be the optimum approach for PL.

The incentive behind EMI is to generalize the covariance model in reducing the impact of coherence estimation error on PL. However, the extra degree of freedom provided by EMI's rank-1 calibration dyadic has been shown to be only marginally successful in improving the performance of phase estimation. A follow-on research direction is to further generalize the covariance model in order to better account for higher rank coherence estimation error. As was the case for EMI, a generalized model would allow a joint estimation of the systematic phase series and the coherence matrix. This research question falls in the realm of classical model selection. The generalization of the model shall be dealt with care, as an increase in model complexity raises the probability of overparameterization. Ergo, further research is necessary for the proposal and validation of new covariance models.

EMI's efficiency has been investigated with respect to the state-of-the-art PL techniques. The comparisons verify EMI as the optimum choice for phase estimation compared with the latter techniques. The incentive behind the proposal of EMI is to advance the state-of-the-art techniques in efficient NRT processing of Big InSAR Data. The Sequential Estimator [1] was our initial proposal for efficient InSAR time series analysis. A further marriage of EMI with the Sequential Estimator is expected to enhance the performance of phase estimation in the support of NRT processing of Big Data. The integration of these two approaches and investigation of the (possible) gained efficiency is a topic for follow-on research.

APPENDIX A

This appendix is dedicated to the derivation of the analytical solution of MLE following the minimization of (10). To solve this optimization, the following gradient is sought for finding the extremum:

$$\begin{aligned} \frac{\partial \text{I}}{\partial \boldsymbol{\zeta}^H} + \frac{\partial \text{II}}{\partial \boldsymbol{\zeta}^H} &= 0 \\ \text{with } \text{I} &:= \alpha^{-2} \boldsymbol{\zeta}^H (\hat{\Gamma}^{-1} \circ \mathbf{C}) \boldsymbol{\zeta} \\ \text{and } \text{II} &:= -\sum_{i=1}^n \ln(|\boldsymbol{\zeta}_i|^2) + 2n\ln(2). \end{aligned} \quad (27)$$

Following the calculation of the two gradients, we have:

$$\frac{\partial \text{I}}{\partial \boldsymbol{\zeta}^H} = \alpha^{-2} (\hat{\Gamma}^{-1} \circ \mathbf{C}) \boldsymbol{\zeta}$$

and

$$\left(\frac{\partial \text{II}}{\partial \boldsymbol{\zeta}^H} \right)_k = -\frac{(\boldsymbol{\zeta})_k}{\sigma_k^{-2}}. \quad (28)$$

Substituting (28) into (27), the estimate of $\hat{\boldsymbol{\xi}}$ yields

$$(\hat{\Gamma}^{-1} \circ C) \hat{\boldsymbol{\xi}} = \alpha^2 \hat{\boldsymbol{\sigma}}^2 \circ \hat{\boldsymbol{\xi}}. \quad (29)$$

The estimate of $\hat{\alpha}$ results from

$$\frac{\partial \text{I}}{\partial \alpha} + \frac{\partial \text{II}}{\partial \alpha} = 0 \quad (30)$$

$$\hat{\alpha} = \frac{1}{n} \hat{\boldsymbol{\xi}}^H (\hat{\Gamma}^{-1} \circ C) \hat{\boldsymbol{\xi}}. \quad (31)$$

The analytical solution is different from both PTA and EMI. To provide a recipe for the calculation of the sought parameters, we further expand (29) and arrive at

$$\begin{aligned} \alpha^2 \sigma_k \exp(-j\phi_k) &= \sum_{i=1}^n (\Gamma^{-1} \circ C)_{ki} \sigma_i^{-1} \exp(-j\phi_i) \\ (\alpha^2 \sigma_k - \sigma_k^{-1} (\Gamma^{-1})_{kk}) \exp(-j\phi_k) &= \sum_{\substack{i=1 \\ i \neq k}}^n (\Gamma^{-1} \circ C)_{ki} \sigma_i^{-1} \exp(-j\phi_i). \end{aligned}$$

Pursuing an iterative solution one has the following.

$$\begin{aligned} \text{Let: } r_k &= \sum_{\substack{i=1 \\ i \neq k}}^n (\Gamma^{-1} \circ C)_{ki} \sigma_i^{-1} \exp(-j\phi_i) : \\ \hat{\phi}_k &= \angle(r_k) \\ \alpha^2 \hat{\sigma}_k - \hat{\sigma}_k^{-1} (\Gamma^{-1})_{kk} &= |r_k| \\ \rightarrow \alpha^2 \hat{\sigma}_k^2 - |r_k| \hat{\sigma}_k - (\Gamma^{-1})_{kk} &= 0 \\ \rightarrow \hat{\sigma}_k &= \frac{|r_k| \pm \sqrt{|r_k|^2 + 4\alpha^2 (\Gamma^{-1})_{kk}}}{2}. \end{aligned} \quad (32)$$

Note that following the positive definiteness of Γ and consequently Γ^{-1} , $(\Gamma^{-1})_{kk} > 0$; hence, the existence of two solutions to (32) is guaranteed. To find a unique solution, $\boldsymbol{\sigma}$ vector with lower norm is preferred for the MLE.

For $\boldsymbol{\sigma} = \vec{\mathbf{1}}$ to hold, the following condition will be met: $|r_k| = 2 - 2\alpha^2 (\Gamma^{-1})_{kk}$. In the cases where this condition holds, the solution of PTA is in fact MLE.

APPENDIX B

Following the probabilistic approach to PL, the optimum metric for weighting the interferograms in estimation of the sought phase series is given by $\Gamma^{-1} \circ \Gamma$. Under this metric, PL is translated into finding the complex vector, which minimizes the objective function $\mathbf{e}^H (\Gamma^{-1} \circ \Gamma \circ I_\Omega) \mathbf{e}$. The additional constraints that each PTA and EMI impose on the sought vector \mathbf{e} to approach this optimization were reviewed in this paper.

The mentioned metric of $\Gamma^{-1} \circ \Gamma$ possesses mathematical features worthy of remark [36]. The elements of this matrix are given by [37]

$$(\Gamma^{-1} \circ \Gamma)_{ik} = \frac{\Gamma_{ik}}{\det(\Gamma)} \gamma_{ik}. \quad (33)$$

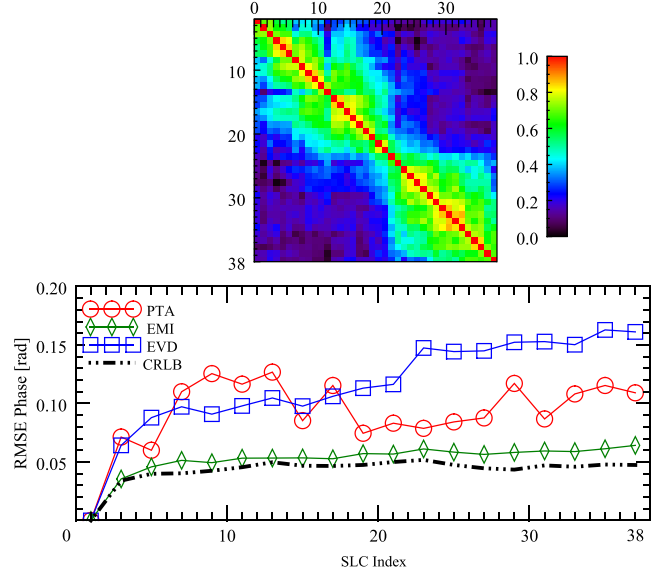


Fig. 14. Performance assessment of different PL estimators compared with CRLB simulated with a coherence matrix over the volcanic caldera for which PTA fails in phase estimation. (Top) Coherence matrix used for simulation. (Bottom) RMSE of phase estimation for a simulated stack of 38 images under the CCG statistic. This analysis further validates the optimality of EMI among the PL estimators.

Here, γ_{ik} is the (i, j) cofactor of matrix Γ defined by

$$\gamma_{ik} = (-1)^{i+j} \Gamma(i|j) \quad (34)$$

where $\Gamma(i|j)$ is the first minor of Γ , as the determinant of the submatrix formed by the elimination of row i and column k of matrix Γ . Summation of the cofactor matrices yields the Laplace expansion, which reads as

$$\det(\Gamma) = \sum_{i=1}^n \Gamma_{ik} \gamma_{ik}. \quad (35)$$

Substituting (35) into (33), it is observed that the product $\Gamma^{-1} \circ \Gamma$ is a quasi-bistochastic matrix, i.e.,

$$\sum_{i=1}^n (\Gamma^{-1} \circ \Gamma)_{ik} = \sum_{k=1}^n (\Gamma^{-1} \circ \Gamma)_{ik} = 1. \quad (36)$$

The quasi-bistochastic property entails that

$$(\Gamma^{-1} \circ \Gamma) \mathbf{e} = \mathbf{e}$$

with

$$\mathbf{e} = \frac{1}{\sqrt{n}} \vec{\mathbf{1}}. \quad (37)$$

The latter introduces $\lambda = 1$ and \mathbf{e} as the minimum eigenvalue and eigenvector of the matrix under study. This eigenvector coincides with the normalized modulus of the PTA model.

Note that the bistochastic property and the respective inference on the minimum eigenvector hold for the matrix $\Gamma^{-1} \circ \Gamma$. Recurring to the product $\Gamma^{-1} \circ \Gamma \circ I_\Omega$ in the objective function of MLE, the observed interferograms of I_Ω violate the bistochastic property, rendering the optimum choice of minimizing vector deviant from $\vec{\mathbf{1}} \exp(j\phi)$.

APPENDIX C

PTA has been observed to perform poorly over the volcanic caldera. In order to investigate its behavior, a frequently observed coherence structure over the volcanic caldera for which PTA fails, while EMI and EVD are both successful is studied here. The estimated coherence Γ is used to simulate a stack of 38 images under the CCG statistics (according to Section III). The coherence matrix and the RMSE of phase estimation for PTA1, EVD, and EMI are provided in Fig. 14. The convergence rate of PTA1 in this restricted simulation scenario is 89%. It, however, decreases to 13.6%, when including the observed phases from real data in I_Ω to the simulations. From this and similar analysis over other parts of the volcanic caldera, it is concluded that the odd behavior of PTA is related to the phase and possible violation of CCG statistics. Further in-depth investigations are required to prove the relation to the latter. This investigated coherence structure is as well shown to affect the efficiency of the estimators and further validates the optimality of EMI among the PL estimators.

ACKNOWLEDGMENT

The authors would like to thank colleagues from the German Aerospace Center (DLR): Dr. R. Shau for the preparation of Sentinel-1 Data and F. Rodriguez Gonzalez for the fruitful discussions. The InSAR processing of Sentinel-1 data is performed with DLR's InSAR wide area processing chain [38].

REFERENCES

- [1] H. Ansari, F. De Zan, and R. Bamler, "Sequential estimator: Toward efficient InSAR time series analysis," *IEEE Trans. Geosci. Remote Sens.*, vol. 55, no. 10, pp. 5637–5652, Oct. 2017.
- [2] S. Tebaldini and A. Monti Guarneri, "Methods and performances for multi-pass SAR interferometry," in *Geoscience and Remote Sensing New Achievements*, P. Imperatore and D. Riccio, Eds. Rijeka, Croatia: InTech, Feb. 2010, doi: [10.5772/9112](https://doi.org/10.5772/9112).
- [3] R. F. Hanssen, *Radar Interferometry: Data Interpretation and Error Analysis* (Remote Sensing and Digital Image Processing). Dordrecht, The Netherlands: Kluwer, 2010.
- [4] H. A. Zebker and J. Villasenor, "Decorrelation in interferometric radar echoes," *IEEE Trans. Geosci. Remote Sens.*, vol. 30, no. 5, pp. 950–959, Sep. 1992.
- [5] A. Ferretti, C. Prati, and F. Rocca, "Permanent scatterers in SAR interferometry," *IEEE Trans. Geosci. Remote Sens.*, vol. 39, no. 1, pp. 8–20, Jan. 2001.
- [6] B. M. Kampes, *Radar Interferometry Persistent Scatterer Technique*. Dordrecht, The Netherlands: Springer, 2006.
- [7] R. Lanari, O. Mora, M. Manunta, J. J. Mallorqui, P. Berardino, and E. Sansosti, "A small-baseline approach for investigating deformations on full-resolution differential SAR interferograms," *IEEE Trans. Geosci. Remote Sens.*, vol. 42, no. 7, pp. 1377–1386, Jul. 2004.
- [8] A. M. Guarneri and S. Tebaldini, "On the exploitation of target statistics for SAR interferometry applications," *IEEE Trans. Geosci. Remote Sens.*, vol. 46, no. 11, pp. 3436–3443, Nov. 2008.
- [9] A. Ferretti, A. Fumagalli, F. Novali, C. Prati, F. Rocca, and A. Rucci, "A new algorithm for processing interferometric data-stacks: SqueeSAR," *IEEE Trans. Geosci. Remote Sens.*, vol. 49, no. 9, pp. 3460–3470, Sep. 2011.
- [10] F. De Zan, F. Rocca, and A. Rucci, "PS processing with decorrelating targets," in *Proc. Envisat Symp.*, Jul. 2007, pp. 1–5.
- [11] G. Fornaro, S. Verde, D. Reale, and A. Pauciullo, "CAESAR: An approach based on covariance matrix decomposition to improve multibaseline–multitemporal interferometric SAR processing," *IEEE Trans. Geosci. Remote Sens.*, vol. 53, no. 4, pp. 2050–2065, Apr. 2015.
- [12] N. Cao, H. Lee, and H. C. Jung, "A phase-decomposition-based PSInSAR processing method," *IEEE Trans. Geosci. Remote Sens.*, vol. 54, no. 2, pp. 1074–1090, Feb. 2016.
- [13] F. De Zan, M. Zonno, and P. Lopez-Dekker, "Phase inconsistencies and multiple scattering in SAR interferometry," *IEEE Trans. Geosci. Remote Sens.*, vol. 53, no. 12, pp. 6608–6616, Dec. 2015.
- [14] S. Samiei-Esfahany and P. Lopez-Dekker, "On the effect of soil moisture phase inconsistencies on phase estimators from distributed scatterers in InSAR stacks," presented at the ESA Fringe Workshop, Helsinki, Finland, Jun. 2017.
- [15] N. Cao, H. Lee, and H. C. Jung, "Mathematical framework for phase-triangulation algorithms in distributed-scatterer interferometry," *IEEE Geosci. Remote Sens. Lett.*, vol. 12, no. 9, pp. 1838–1842, Sep. 2015.
- [16] A. M. Guarneri and S. Tebaldini, "Hybrid Cramér–Rao bounds for crustal displacement field estimators in SAR interferometry," *IEEE Signal Process. Lett.*, vol. 14, no. 12, pp. 1012–1015, Dec. 2007.
- [17] Y. Wang and X. X. Zhu, "Robust estimators for multipass SAR interferometry," *IEEE Trans. Geosci. Remote Sens.*, vol. 54, no. 2, pp. 968–980, Feb. 2016.
- [18] H. Ansari, F. De Zan, N. Adam, K. Goel, and R. Bamler, "Sequential estimator for distributed scatterer interferometry," in *Proc. IEEE Geosci. Remote Sens. Symp.*, Beijing, China, Jul. 2016, pp. 6859–6862.
- [19] S. Samiei-Esfahany, J. E. Martins, F. van Leijen, and R. F. Hanssen, "Phase estimation for distributed scatterers in InSAR stacks using integer least squares estimation," *IEEE Trans. Geosci. Remote Sens.*, vol. 54, no. 10, pp. 5671–5687, Oct. 2016.
- [20] R. Touzi, A. Lopes, J. Bruniquel, and P. W. Vachon, "Coherence estimation for SAR imagery," *IEEE Trans. Geosci. Remote Sens.*, vol. 37, no. 1, pp. 135–149, Jan. 1999.
- [21] R. Bamler and P. Hartl, "Synthetic aperture radar interferometry," *Inverse Problems*, vol. 14, no. 4, pp. R1–R54, Aug. 1998.
- [22] A. Ferretti, A. Fumagalli, F. Novali, F. De Zan, A. Rucci, and S. Tebaldini, "Process for filtering interferograms obtained from SAR images acquired on the same area," U.S. Patent 8 711 029 B2, Apr. 29, 2014.
- [23] F. Casu *et al.*, "SBAS-DInSAR parallel processing for deformation time-series computation," *IEEE J. Sel. Topics Appl. Earth Observ. Remote Sens.*, vol. 7, no. 8, pp. 3285–3296, Aug. 2014.
- [24] N. R. Goodman, "Statistical analysis based on a certain multivariate complex Gaussian distribution (an introduction)," *Ann. Math. Statist.*, vol. 34, no. 1, pp. 152–177, 1963.
- [25] E. Anderson *et al.*, *LAPACK Users' Guide*, 3rd ed. Philadelphia, PA, USA: SIAM, Jan. 1999, doi: [10.1137/1.9780898719604](https://doi.org/10.1137/1.9780898719604).
- [26] I. S. Dhillon, B. N. Parlett, and C. Vömel, "The design and implementation of the MRRA algorithm," *ACM Trans. Math. Softw.*, vol. 32, no. 4, pp. 533–560, Dec. 2006.
- [27] A. Parizzi, X. Cong, and M. Eineder, "First results from multifrequency interferometry—A comparison of different decorrelation time constants at L, C, and X Band," in *ESA Scientific Publications*, 2009, pp. 1–5.
- [28] F. De Zan and P. López-Dekker, "SAR image stacking for the exploitation of long-term coherent targets," *IEEE Geosci. Remote Sens. Lett.*, vol. 8, no. 3, pp. 502–506, May 2011.
- [29] A. Parizzi and R. Brćic, "Adaptive InSAR stack multilooking exploiting amplitude statistics: A comparison between different techniques and practical results," *IEEE Geosci. Remote Sens. Lett.*, vol. 8, no. 3, pp. 441–445, May 2011.
- [30] A. M. Zoubir, V. Koivunen, Y. Chakhchoukh, and M. Muma, "Robust estimation in signal processing: A tutorial-style treatment of fundamental concepts," *IEEE Signal Process. Mag.*, vol. 29, no. 4, pp. 61–80, Jul. 2012.
- [31] P. J. Huber and E. M. Ronchetti, *Robust Statistics*. 2nd ed. Hoboken, NJ, USA: Wiley, 2009.
- [32] F. R. Hampel, "The influence curve and its role in robust estimation," *J. Amer. Statist. Assoc.*, vol. 69, no. 346, pp. 383–393, 1974.
- [33] P. J. Rousseeuw and C. Croux, "Alternatives to the median absolute deviation," *J. Amer. Statist. Assoc.*, vol. 88, no. 424, pp. 1273–1283, Dec. 1993.
- [34] C.-A. Deledalle, L. Denis, F. Tupin, A. Reigber, and M. Jäger, "NL-SAR: A unified nonlocal framework for resolution-preserving (Pol)(In)SAR denoising," *IEEE Trans. Geosci. Remote Sens.*, vol. 53, no. 4, pp. 2021–2038, Apr. 2015.
- [35] M. Schmitt, J. L. Schönberger, and U. Stilla, "Adaptive covariance matrix estimation for multi-baseline InSAR data stacks," *IEEE Trans. Geosci. Remote Sens.*, vol. 52, no. 11, pp. 6807–6817, Nov. 2014.
- [36] G. P. Styan, "Hadamard products and multivariate statistical analysis," *Linear Algebra Appl.*, vol. 6, pp. 217–240, 1973.

- [37] R. Bru, M. T. Gassó, I. Giménez, and J. A. Scott, "The Hadamard product of a nonsingular general H-matrix and its inverse transpose is diagonally dominant," *J. Appl. Math.*, vol. 2015, May 2015, Art. no. 264680.
- [38] N. Adam, F. R. Gonzalez, A. Parizzi, and R. Breic, "Wide area persistent scatterer interferometry: Current developments, algorithms and examples," in *Proc. IEEE Geosci. Remote Sens. Symp.*, Jul. 2013, pp. 1857–1860.



Homa Ansari received the B.Sc. degree in geodesy and geodetic engineering from the University of Isfahan, Isfahan, Iran, in 2011, and the M.Sc. degree (*cum laude*) in earth-oriented space science and technology from the Technical University of Munich, Munich, Germany, in 2013, with specialization on the global navigation satellite systems and microwave remote sensing. She is currently pursuing the Ph.D. degree with the Remote Sensing Technology Institute, German Aerospace Center (DLR), Weßling, Germany.

In 2012, she joined the German Geodetic Research Institute, Munich, as a Research Assistant. She joined DLR as a Research Assistant in 2013. Since 2014, her Ph.D. work at DLR has been contributing to the German Helmholtz Alliance on Remote Sensing and Earth System Dynamics as well as the studies of the Tandem-L mission. In 2017, she visited the Department of Geoscience and Remote Sensing, Delft University of Technology, Delft, The Netherlands, as a Visiting Researcher. Her research interests include statistical signal processing, estimation theory, and geodetic time series analysis with applications to the advancement of differential SAR interferometry.

Ms. Ansari was a recipient of the IEEE Mikio Takagi Prize, awarded for the Best Student Paper at the 2017 IEEE International Geoscience and Remote Sensing Symposium, TX, USA, in 2017.



Francesco De Zan was born in Lodi, Italy, in 1979. He received the master's degree in telecommunications engineering from the Politecnico di Milano, Milan, Italy, in 2004, with a focus on signal processing and remote sensing, and the Ph.D. degree from the Politecnico di Milano in 2008, with a focus on synthetic aperture radar (SAR) interferometry with distributed and decorrelating.

He has contributed to the development of the TOPS acquisition mode, which is currently used on ESA Sentinel-1 satellites, and collaborated with T.R.E., Milan. In 2007, he joined the Stanford Exploration Group, Stanford University, Stanford, CA, USA, as a Visiting Researcher. He joined the German Aerospace Center, Weßling, Germany, in 2008, where he was with the Microwave and Radar Institute and then with the Remote Sensing Technology Institute, contributing to the development of the Tandem-L mission concept. He was involved in aspects related to acquisition planning, performance models for deformation retrieval with InSAR and SAR tomographic applications, orbit design, the calibration of the TanDEM-X interferometer, and discovering and explaining interferometric effects which were hampering the quality of the DEM products. He was also involved in several projects for the European Space Agency related to mission design, commissioning, and application development for SAR satellites. His research interests include SAR including the performance of phase and delay estimators, ionospheric propagation estimation, focusing and precise geolocation of targets, soil moisture and vegetation effects, and inconsistencies in SAR interferometric phases.



Richard Bamler (M'95–SM'00–F'05) received the Diploma degree in electrical engineering, the Ph.D. degree in engineering, and the Habilitation degree in signals and systems theory from the Technical University of Munich (TUM), Munich, Germany, in 1980, 1986, and 1988, respectively.

He was with TUM from 1981 to 1989, where he was involved in optical signal processing, holography, wave propagation, and tomography. He joined the German Aerospace Center (DLR), Weßling, Germany, in 1989, where he is currently the Director of the Remote Sensing Technology Institute. In 1994, he joined the Jet Propulsion Laboratory, Pasadena, CA, USA, as a Visiting Scientist, where he was involved in the preparation of the SIC-C/X-SAR missions, and in 1996, he joined the University of Innsbruck, Innsbruck, Austria, as a Guest Professor. Since 2003, he has been a Full Professor in remote sensing technology with TUM as a double appointment with his DLR position. His teaching activities include university lectures and courses on signal processing, estimation theory, and synthetic aperture radar (SAR). He, his team, and his institute have been involved in SAR and optical remote sensing, image analysis and understanding, machine learning, stereo reconstruction, computer vision, ocean color, hyperspectral image analysis, passive and active atmospheric sounding, and laboratory spectrometry. They were and are responsible for the development of the operational processors for SIC-C/X-SAR, SRTM, TerraSAR-X, TanDEM-X, PAZ, Tandem-L, ERS-2/GOME, ENVISAT/SCIAMACHY, MetOp/GOME-2, Sentinel 5p, Sentinel 4, DESIS, and EnMAP. His research interests include algorithms for optimum information extraction from remote sensing data; this involves new estimation algorithms, such as sparse reconstruction and compressive sensing for SAR, multispectral/hyperspectral imaging, data fusion, and machine learning.